Journal of Cluster Science (2020) 31:355–366
https://doi.org/10.1007/s10876-019-01649-x

ORIGINAL PAPER

Nano Biomedical Potential of Biopolymer Chitosan-Capped Silver Nanoparticles with Special Reference to Antibacterial, Antibiofilm, Anticoagulant and Wound Dressing Material

Sekar Vijayakumar[1,2] · Balasubramanian Malaikozhundan[1,3] · Ayyanar Parthasarathy[1] · Kandasamy Saravanakumar[2] · Myeong-Hyeon Wang[2] · Baskaralingam Vaseeharan[1]

Received: 21 May 2019 / Published online: 6 August 2019

Abstract

Silver nanoparticles have been widely used to treat bacterial infections on wounds. Chitosan is a natural polymer having good biocompatibility and biodegradability. Chitosan have antibacterial effects and are largely used in healthcare practices to cure wounds. In this scenario, an attempt was made to biologically synthesize AgNPs using the chitosan extracted from shrimp shell waste. The synthesized Ch-AgNPs exhibited strong UV absorption spectra at 404 nm. XRD spectrum confirmed the presence of nanocrystals with an average crystallite size of 26 nm. HR-TEM images have shown spherical shaped particles with the size ranging between 10 and 50 nm. Ch-AgNPs exhibited antibacterial activity in a dose-dependent manner and greater activity was observed against *P. aeruginosa*. The zone of inhibition against *P. aeruginosa* was 10, 15 and 20 mm at 25, 50 and 100 μg mL^{-1}, respectively. The zone of inhibition against MRSA was 8, 15 and 18 mm at 25, 50 and 100 μg mL^{-1} respectively. Ch-AgNPs effectively inhibited the biofilm of *MRSA* and *P. aeruginosa* at 100 μg mL^{-1}. In addition, Ch-AgNPs coated band-aid cloth showed greater antibacterial activity compared to uncoated band-aid cloth. Furthermore, Ch-AgNPs exhibited anticoagulant activity by inhibiting the coagulation of human blood for 24 h.

Keywords Chitosan · Ag NPs · Wound pathogens · Biofilms · Anticoagulant · Wound dressing material

Introduction

Wound including those resulting from burns often provide a favorable environment for the colonization of microorganisms which cause infection (bacterial or fungal) and in turn may delay wound healing [1]. The microorganisms can exist in both the planktonic (free-living) and biofilm phenotypic states, with the latter being predominant in all medical and natural environments [2]. Both phenotypic states may play an important role in impairing healing and causing infection of both acute and chronic wounds [2]. However, it is the biofilm phenotypic state that is more fundamental in preventing chronic wounds from healing in a timely manner [2]. Biofilms are defined as a community of microorganisms that are attached to a surface or a group

Sekar Vijayakumar and Ayyanar Parthasarathy are first author equally contributed.

Electronic supplementary material The online version of this article (https://doi.org/10.1007/s10876-019-01649-x) contains supplementary material, which is available to authorized users.

✉ Myeong-Hyeon Wang
mhwang@kangwon.ac.kr

✉ Baskaralingam Vaseeharan
vaseeharanb@gmail.com;
vaseeharanb@alagappauniversity.ac.in

[1] Nanobiosciences and Nanopharmacology Division, Biomaterials and Biotechnology in Animal Health Lab, Department of Animal Health and Management, Science Campus 6th Floor, Alagappa University, Karaikudi, Tamil Nadu 630004, India

[2] Natural Product Biomedical Technology Laboratory, Department of Medical Biotechnology, College of Biomedical Sciences, Kangwon National University, Chuncheon, Gangwon-do 24341, Republic of Korea

[3] Department of Biology, The Gandhigram Rural Institute (Deemed to be University), Gandhigram, Dindigul District 624 302, Tamil Nadu, India

of microorganisms themselves forming microbial aggregates, which are encased within an extracellular matrix of polysaccharides, proteins and glycoproteins, referred to as the extracellular polymeric substance (EPS). Within the attached state, microorganisms have the ability to create an environment conducive for their protection and longevity [3]. The wound infections caused by biofilms are a difficult clinical microbiological diagnosis and cause of treatment failure [4]. Biofilms have detrimental effects on wound healing by affecting healing times, risk of infection and costs to the health service [5]. Wound biofilms represent a challenge to the microbiological diagnosis as well as to the treatment, requiring new and rapid detection methods and combined approaches, such as mechanical debridement and administration of systemic or topical antimicrobial agents, and antibiotics or other alternative anticipatory or healing approaches [6].

Modern wound dressings and topical treatments like ointments and creams are used to assist the treatment of the wound bed, however, their frequent application and the need for repeated washing of wound initiates pain and patient discomfort [7]. Nano-bioactive dressings play a role beyond the interactive dressings in the process of healing. Biopolymer drug capped nano-materials have been recently introduced as a novel combination with enhanced biochemical stuffs unveiling unique drug delivery carrier. Natural polymer chitosan has received a great deal of attention due to their well-documented biocompatibility, biodegradable, low toxicity [8] and degradability by human enzymes [9]. Other important characteristics are that chitosan exhibits structural similarity to the extracellular matrix molecules, as well as the formation of stable complexes with its molecules and in addition its antimicrobial activity [10, 11]. For these reasons the chitosan has been approved by the FDA to be used in wound dressings [12].

Silver nanoparticles (AgNPs) is one of the most prominent nanoproducts for medical purposes, due to their strong antimicrobial activity. Wound dressings, contraceptive devices, surgical instruments and bone prostheses coated or embedded with nanosilver is available [13]. The purpose of this investigation is to synthesize chitosan coated silver nanoparticles (Ch-AgNPs). The in vitro antibacterial and antibiofilm activities of Ch-AgNPs were evaluated against wound infection causing Gram-positive methicillin-resistant *S. aureus* and Gram-negative *P. aeruginosa.* Furthermore, Ch-AgNPs coated wound dressing biomaterial (clinical band-aid cloth) was tested against wound infection causing methicillin-resistant *S. aureus* and *P. aeruginosa.* In addition, the in vitro anticoagulant activity of Ch-AgNPs was investigated using human blood.

Materials and Methods

Chemicals and Reagents Used

Silver nitrate ($AgNO_3$) (ACS reagent, $\geq$ 99.0%), chitosan (isolation from shrimp shells, deacetylated), sodium borohydride ($NaBH_4$) ($\geq$ 98.0), ninhydrin (N4876), acetic acid (CH_3COOH) (ACS reagent, $\geq$ 99.7%), sodium dodecyl sulfate (SDS) (L3771), phenol (P1037), Nacl (746398), H_2SO_4 (339741), methicillin antibiotic, Whatman filter paper (WHA10348903), phosphate buffered saline (PBS) tablets (pH 7.4), acridine orange (235474) and crystal violet (C3886) were purchased from Sigma Aldrich, India. Nutrient broth (NB) and Mueller–Hinton Agar (MHA) were purchased from HiMedia (India). Gram-positive methicillin-resistant *S. aureus* (MRSA-ATCC 33591) and Gram-negative *P. aeruginosa* (ATCC-27853) bacteria were commercially purchased from American type culture collection (ATCC). Ultra-pure deionized water from PURITE (18 MΩ) system was used in all the experiments. The chemicals used were of analytical grade. The glass wares used for experimental purposes were properly washed, sanitized and autoclaved.

Isolation of Chitosan

The shells of Indian white shrimp, *Fenneropenaeus indicus* were collected from the Thondi coast, Tamil Nadu, India. About 250 g of shrimp shells were washed thoroughly with water and dried to remove excess water. Then, the dried shells were demineralized using 1 N HCl (1:15 w/v) at ambient temperature (approximately 30 °C) for 6 h. The residue was washed with distilled water until pH reached to 6.5–7 and then the residue was dried. After that, the demineralized shrimp shells were deproteinized using 3.5% NaOH solution (1:10 w/v) at 65 °C for 2 h and decoloration was done with NaOCl (0.315%). Then, the residue was washed thoroughly with water, followed by distilled water until the pH reached 6.5–7.5. The chitin was dried, ground and screened. The chitin obtained from the above process was deacetylated in 50% NaOH (1:10 w/v) for 5 h at 100 °C. After deacetylation, the chitosan was washed thoroughly with water, followed by distilled water. They were then oven dried at 120 °C for 24 h to obtain 10 g of creamy white powder [14].

Synthesis and Purification of Chitosan Coated AgNPs (Ch-AgNPs)

Ch-AgNPs were synthesized according to the previously described method [15]. Chitosan solution (0.2%w/v) was prepared in 1% acetic acid and filtered through 0.22 μm

Millipore syringe filter to eliminate insoluble fractions. $AgNO_3$ solution (20 mL, 0.01 M) was mixed with 470 mL of 0.2% (w/v) chitosan at 50 °C and stirred for 30 min. To this mixture, 10 mL of freshly prepared sodium borohydride ($NaBH_4$) was added and again stirred for 90 min till a clear yellow to brown color was observed. The synthesized Ch-AgNPs were purified using refrigerated high-speed centrifuge (Kubota 6500, Japan) at 17,000×*g* (rotor model AG-506R-36,873) relative centrifugal force (RCF) maintained at 4 °C for 20 min. After centrifugation, AgNPs pellets were suspended in deionized water and centrifuged thrice in the same manner to ensure complete removal of extraneous matter. Finally, purified nano-silver colloidal dispersion was collected, sterilized by filtration (0.22 µm syringe filter), lyophilized and stored at room temperature for further use [16].

Physico-Chemical Characterization of Ch-AgNPs

The physico-chemical characterization of Ch-AgNPs were analyzed through UV–vis spectroscopy (UV-1800, Shimadzu, Japan), X-ray diffraction (XRD) (X'PERT PRO PAN analytical, PHILIPS, USA), Fourier transform infrared (FTIR) spectroscopy (Shimadzu, Japan), high resolution transmission electron microscopy (HR-TEM) (JOEL model instrument 1200 EX instrument, Japan), and energy dispersive X-ray analysis (EDX).

UV–Visible Spectroscopy Analysis

The optical absorption of the Ch-AgNPs reaction mixture (1 mL aliquots) was measured at regular intervals to monitor the bioreduction of Ag^+ ions. UV–Vis spectra were monitored as the function of time of reaction on a spectrophotometer over the range of 300–500 nm operated at a resolution of 1 nm [17].

X-ray Diffraction (XRD) Analysis

The synthesized Ch-AgNPs was dispersed in distilled water via sonication for 30 min and subsequently centrifuged at 9000×*g* for 30 min to remove any unbound ligand. They were then freeze-dried and lyophilized to obtain powdered Ch-AgNPs. The particle size and crystalline nature of the powdered Ch-AgNPs were determined using XRD with a powder diffractometer operating at a voltage of 50 kV and a current of 30 mA. The crystalline size of silver nanoparticles was determined using Debye–Scherrer's equation.

$$D = 0.9\lambda/\beta\cos\theta$$

where λ is the X-ray wavelength, β is the full width half-maximum (FWHM) of the Ag (111) line and θ is the diffraction angle [18].

Fourier Transform Infrared (FTIR) Spectroscopic Analysis

FTIR was performed following the method of Chandran et al. [19]. Two milligrams of Ch-AgNPs was mixed with 200 mg potassium bromide (FTIR grade) and pressed into a pellet. FTIR spectra of the sample pellet were recorded in FTIR spectroscopy at a resolution of 4 cm^{-1}.

High-Resolution Transmission Electron Microscopy (HR-TEM) and Energy Dispersive X-ray (EDX) Analysis

The size and surface morphology of Ch-AgNPs was determined using HR-TEM following the method described by Deepak et al. [20]. HR-TEM analysis was performed by placing a small volume of Ch-AgNPs on carbon-coated copper grids and the solvent was allowed to evaporate for 30 min. The presence of elemental silver was determined using EDX Zeiss Evo 50 equipped with HR-TEM [20].

Quantitative Determination of Chitosan in Ch-AgNPs

Quantitative determination of chitosan in Ch-AgNPs was done according to Jena et al. [21]. Ninhydrin reagent was prepared by dissolving ninhydrin (0.5 g) in isopropanol (30 mL). The resulting solution was mixed with 20 mL of sodium acetate buffer (pH 5.5). A chitosan standard curve ranging from 10 to 1 mg mL^{-1} was generated, and this was used to calculate the quantity of chitosan present in freshly prepared (day 1) and old (day 30) Ch-AgNPs. Ninhydrin reagent (1 mL) was added to test samples (1 mL) and boiled for 30 min. The solution was then cooled to 30 °C and diluted with 50% ethanol (5 mL). The absorbance was measured at 570 nm on UV–Visible spectrophotometer (UV-1800; Shimadzu, Japan).

Stability of Ch-AgNPs

Long-term stability of Ch-AgNPs was determined by visual inspection after 1-month storage at 4 °C followed by UV–vis spectroscopic analysis and antibacterial studies following agar well diffusion method [22].

Nano Biomedical Potential of Biopolymer Chitosan-Capped Silver Nanoparticles

In Vitro Antibacterial Assay

The agar well diffusion method [23] was used to screen the antibacterial activity of Ch-AgNPs against wound infection

causing Gram-positive methicillin-resistant *S. aureus* and Gram-negative *P. aeruginosa* bacteria. Briefly, the MHA plates were prepared by pouring 15 mL of molten media into sterile petri plates. The plates were allowed to solidify and 0.1% suspension of bacterial strains were swabbed uniformly and the inoculum was allowed to dry for 5 min. Wells were punched aseptically using a sterile cork borer on the plate. Then, 50 µL of Ch-AgNPs, bare $AgNO_3$ and bare chitosan was loaded into the wells at different concentration (25, 50, and 100 µg mL^{-1}). The compound was allowed to diffuse for 5 min and the plates were incubated at 37 °C for 24 h. The antibacterial efficacy of Ch-AgNPs was compared with bare $AgNO_3$ and bare chitosan. The inhibition zones formed around the wells were measured with a transparent ruler in millimeter.

Minimum Inhibitory Concentration (MIC) of Ch-AgNPs

The MIC was evaluated by broth micro dilution method on 96-well plate method described by CLSI [24]. Different concentrations of Ch-AgNPs were added on the plate wells containing Mueller–Hinton broth (MHB). The positive control was considered the well with inoculum in MHB and negative control only MHB with saline. The experimental was performed in triplicates. After the process, the plate was incubated for 24 h at 37 °C. The MIC was considered as the lowest concentration of Ch-AgNPs giving a complete inhibition of visible bacterial growth in comparison with a control well after incubation at 37 °C for 24 h.

Antibacterial Activity of Ch-AgNPs Coated Clinical Band-Aid Cloth (Cheese Cloth)

The antibacterial activity of Ch-AgNPs coated clinical band-aid cloth (cheese cloth) was determined according to the procedure by Sankaranarayanan et al. [25]. Briefly, clinical band-aid cloth was purchased from the medical shop and it was sterilized by moist heat. After sterilization, the clinical band-aid cloth was dried and exposed to ultraviolet radiation for 15 min. The sterilized clinical band-aid cloth was coated with 100 µg mL^{-1} of Ch-AgNPs by dip coating method. Fresh culture of Gram-positive MRSA and Gram-negative *P. aeruginosa* was swabbed on sterilized Mueller–Hinton Agar (MHA) plates to which Ch-AgNPs coated clinical band-aid cloth was placed and incubated at 37 °C for 24 h. The antibacterial activity of Ch-AgNPs coated clinical band-aid cloth was determined by measuring the inhibition zones formed around the Ch-AgNPs coated clinical band-aid cloth compared to bare $AgNO_3$ and bare chitosan coated clinical band-aid cloth.

Antibiofilm Assay

Bacterial colonies such as MRSA and *P. aeruginosa* (1×10^6 CFU mL^{-1}) were allowed to grow on glass coverslip pieces (dimension 1 × 1 cm) placed in 24-well polystyrene plates with 1 mL nutrient broth along with different concentrations of Ch-AgNPs (25–100 µg mL^{-1}) and incubated at 37 °C for 24 h. The glass coverslip pieces were stained with acridine orange (0.1%). Staining was done after washing the biofilm with PBS and visualized under confocal laser scanning microscope (CLSM-Carl Zeiss LSM 710). Z-stack analysis (surface topography and three-dimensional architecture) was done to measure the biofilm thickness. Glass cover slips were scanned and Z-stacks were acquired at z step-size of 0.388 mm. Each field size was 455 mm by 455 mm at 40× magnification. Microscope images were acquired with the Zen 2009 image software (Carl Zeiss, Germany) [26].

Extracellular Polymeric Substance (EPS) Quantification Assay

Total carbohydrate assay was used to determine the extracellular polymeric substance (EPS) production on the surface of bacteria. Briefly, sterile glass coverslips placed in 24-well polystyrene plates were immersed with the test culture at their BIC and incubated for 24 h.

$$\text{Biofilm Inhibitory percentage} = \frac{(\text{Absorbance of control} - \text{Absorbance of sample})}{\text{Absorbance of control}} \times 100$$

After incubation, the glass coverslips were removed and washed with 0.9% NaCl. The cell suspensions in 0.9% NaCl was transferred to test tubes with an equal volume of 5–7% phenol. Five volumes of concentrated H_2SO_4 containing 0.2% hydrazine sulphate were added. The mixture was incubated in dark for 1 h, and the absorbance was measured at OD 490 nm after centrifugation (10,000×*g*) for 10 min [27].

Biofilm Detachment Assay

The biofilm detachment assay was performed following Davies et al. [28] method with slight modifications. Overnight cultures of MRSA and *P. aeruginosa* (OD at 595 nm = ~ 1.5) were diluted with fresh Auto inducer Bioassay (AB) medium (1:20) in the presence or absence of Ch-AgNPs (1%). The diluted cultures (100 µL) were transferred into a 96-well polystyrene microtiter plate and incubated at 37 °C for 24 h without agitation. 3 µL of sodium dodecyl sulfate (SDS; 10%) was then added to each well, and the mixture was incubated for 30 min.

Absorbance was measured at 595 nm for the suspended cells. For the static biofilm assay, same steps were followed as described above.

Anticoagulant Assay

The anticoagulant assay was carried out following the method described by Kaleeshwaralal et al. [29]. Blood samples from healthy human volunteers (25–32 years old) were used in this study. Siliconized Vacutainer tubes (Becton–Dickinson, Rutherford, NJ) were used to withdraw whole blood. The blood sample was collected in three different tubes containing anti-coagulant heparin (Tube A) or Ch-Ag NPs at 1:0.5% (v/v) (Tube B) or Tube C without any anticoagulant. The ability of Ch-Ag NPs to inhibit the coagulation of blood plasma was examined.

Results and Discussion

Physico-Chemical Characterization of Ch-AgNPs

UV–Visible Spectroscopy

In the present study, AgNPs was synthesized using the chitosan purified from the shrimp shells (*Fenneropenaeus indicus*). The data here reveals that chitosan act as a capping agent in AgNPs synthesis. The UV–Visible spectrophotometer is used to determine the optical and electronic properties of AgNPs [30]. The change in color from pale yellow to brown was observed due to surface plasmon vibrations [31]. In the present study, Ch-AgNPs exhibited strong UV absorption spectra at 404 nm due to its surface plasmon resonance (SPR) (Fig. 1). The broadening of UV–Visible peak suggests that synthesized AgNPs were polydisperse in nature [32]. The present finding corroborates with the results of Tran et al. [33] and Wei et al. [34] who reported that surface plasmon resonance shift increases with increasing concentration of the chitosan.

X-ray Diffraction (XRD) Analysis

X-ray diffraction is used to characterize the crystallographic structure, grain size, and preferred orientation in polycrystalline or powdered samples. This is a preferred method for characterization of unknown crystalline materials [35]. In the present study, the XRD spectrum revealed that the Ch-AgNPs were in the form of nanocrystals as evidenced by the Bragg's reflection peaks 2θ value at 38.42°, 44.36°, 64.40° and 77.49°, which corresponds to lattice planes (111), (200), (220) and (311) of face-centered cubic (FCC) crystal structure of AgNPs respectively

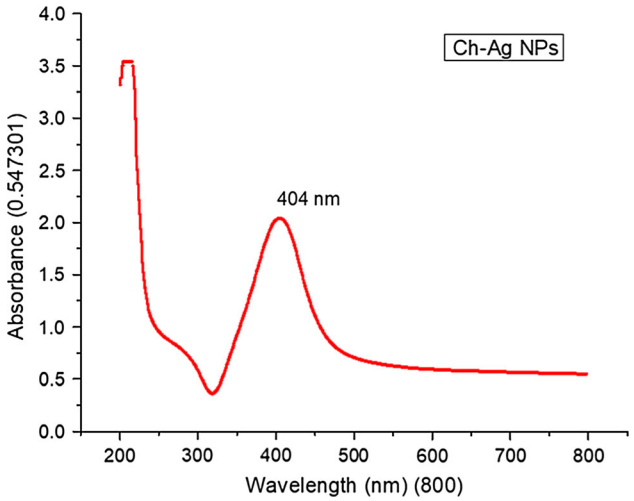

Fig. 1 UV–Vis spectrum showing the surface plasmon resonance of Ch-AgNPs

(Fig. 2). The obtained data matched well with the Joint Committee on Powder Diffraction Standards (JCPDS) file No. 04-0783. The broadening of Bragg's peaks indicates the formation of Ch-AgNPs which was in agreement with the reported data [36]. The average crystalline size of the synthesized Ch-AgNPs as calculated by Scherrer equation was found to be 26 nm.

Fourier Transform Infrared (FTIR) Spectroscopy Analysis

FTIR measurement was carried out to identify the possible biomolecules responsible for capping of Ch-AgNPs. The interaction sites of bare chitosan and AgNPs were characterized by FTIR spectroscopy. The FTIR spectra of the synthesized Ch-AgNPs showed functional groups at 3428, 2925, 1611, 1414, 1305, 1098, 1029, 831 and 624 cm^{-1} (Fig. 3). The intense broad band at 3428 cm^{-1} could be

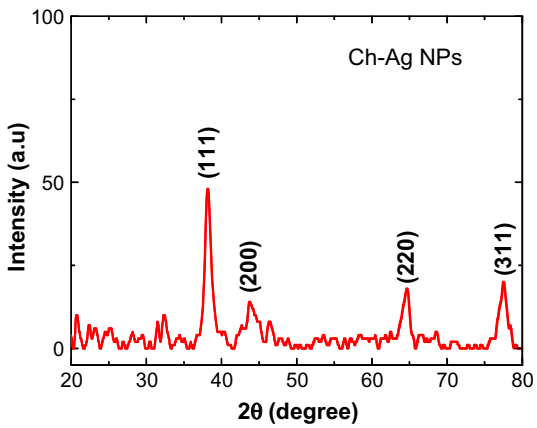

Fig. 2 XRD pattern showing various Bragg's reflection peaks of Ch-AgNPs (JCPDS card No. 04-0783)

due to the stretching of O–H groups. The band observed at 2925 and 1611 cm^{-1} may be due to the stretching of C–H groups. The band at 1414 and 1305 cm^{-1} corresponds to C–C stretching vibrations of aromatic amines [36]. The band at 1098 and 1029 cm^{-1} is characteristic of C–OH stretching of secondary alcohols [30]. The band at 831 and 624 cm^{-1} regions is characteristic of C–H bending vibrations of stabilized silver nanoparticles indicating that chitosan is involved in the process of stabilization. This peak was also found in the FTIR spectrum of chitosan. The results of FTIR support the finding of Balavandy et al. [30] and Namashivayam et al. [31].

High-Resolution Transmission Electron Microscopy (HR-TEM) and Energy Dispersive X-ray (EDX) Analysis

In the present study, high-resolution transmission electron microscopic (HR-TEM) images revealed that the Ch-AgNPs were dispersed and clear spherical particles with particle size ranging from 10 to 50 nm (Fig. 4). These results are in accordance with Dipali et al. [15] who reported that the particle size of chitosan coated AgNPs were between 10 and 50 nm. The elemental composition of Ch-AgNPs determined through EDX showed clear identification peaks of major energies of silver confirming the presence of silver in Ch-AgNPs (Fig. 5). This finding is in agreement with Wei et al. [34].

Quantification of Chitosan

Quantification of chitosan in Ch-AgNPs showed that the amounts of chitosan leached from the freshly prepared (day 1) and (day 30) old Ch-AgNPs were 977.25 and 823.60 μg mL^{-1}, respectively. Similarly, Jena et al. [21] reported that the amount of chitosan in Ch-AgNPs at day 1

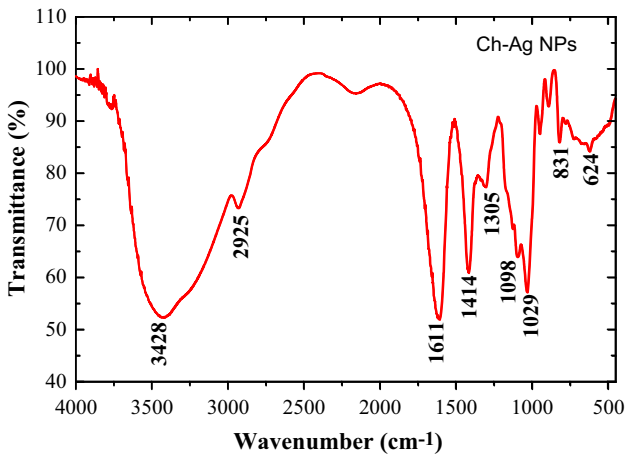

Fig. 3 FTIR spectra of Ch-AgNPs

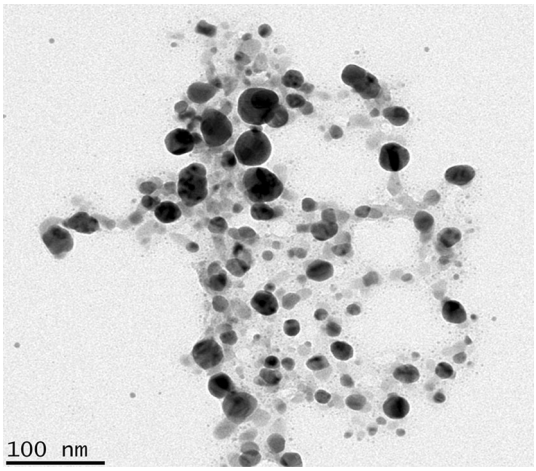

Fig. 4 High-resolution transmission electron microscopic (HR-TEM) images showing the topography and size of Ch-AgNPs

and after 30 days were 987.27 and 813.63 μg mL^{-1}, respectively.

Stability of Ch-AgNPs

After 1 month of synthesis, the Ch-AgNPs were well-dispersed without any agglomeration. Obviously, no change in the color and absorption peak was recorded. These results indicate that the synthesized Ch-AgNPs had good stability even after storage (Supplementary Fig. 1).

Nano Biomedical Potential of Biopolymer Chitosan-Capped Silver Nanoparticles

Minimum Inhibitory Concentration (MIC) of Ch-AgNPs

Minimum inhibitory concentration (MIC) of Ch-AgNPs was comparatively lesser than that of bare $AgNO_3$ and bare chitosan. The MIC of Ch-AgNPs against MRSA and *P. aeruginosa* was 3.78 μg mL^{-1} and 1.84 μg mL^{-1}, respectively (Table 1). Our results are supported by Lima et al. [35] who reported that the AgNPs coated with chitosan induced a potent effect against all tested microorganisms at MICs ranging between 1.69 and 3.38 μg mL^{-1}. These values are lower than the MICs obtained for chitosan and $AgNO_3$ solutions. These findings indicate the synergistic effect of chitosan and $AgNO_3$ on inhibition of microbes when combined as Ch-AgNPs.

In Vitro Antibacterial Activity

The in vitro antibacterial activity of Ch-AgNPs was investigated against Gram-positive MRSA and Gram-negative *P. aeruginosa* bacteria by the agar well diffusion method. The antibacterial activity of Ch-AgNPs was

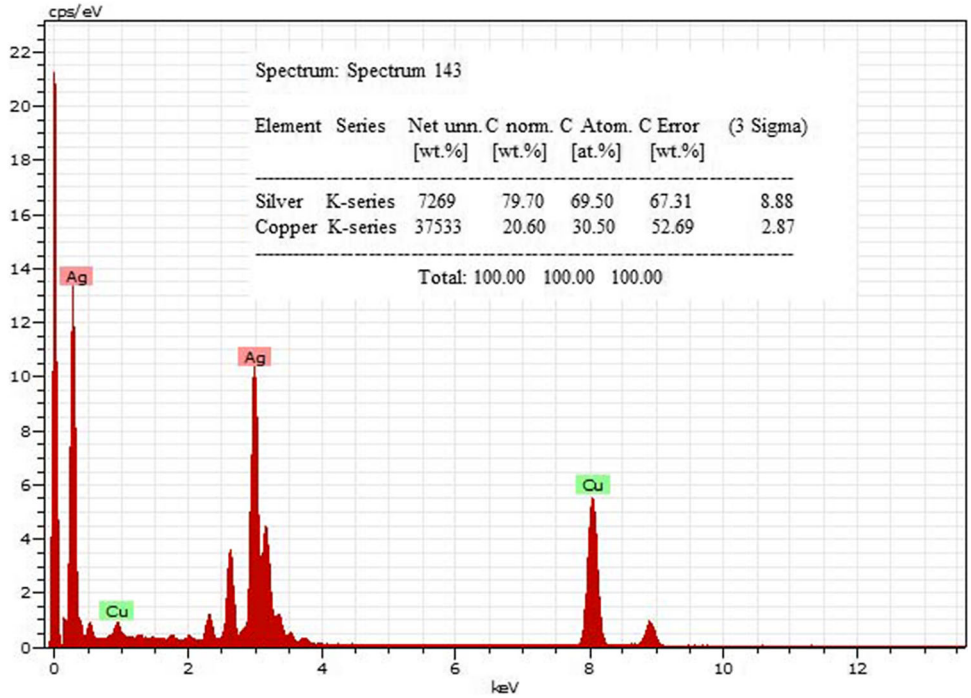

Fig. 5 EDX showing the elemental composition of Ch-AgNPs

Table 1 Minimum inhibitory concentrations (MIC) of Ch-AgNPs in comparison with bare chitosan, bare $AgNO_3$ and methicillin

S. no.	Bacteria	Concentration (μg mL^{-1})*			
		Bare chitosan	Bare $AgNO_3$	Methicillin	Ch-AgNPs
1.	Methicillin resistant *Staphylococcus aureus* (MRSA)	5.10 ± 2.2^a	4.89 ± 1.8^b	0	3.78 ± 1.7^c
2.	*Pseudomonas aeruginosa*	3.84 ± 1.8^a	2.65 ± 1.4^b	–	1.84 ± 0.17^c

* Values are mean ± SE of three replicates. Within each column, different letters indicate significant differences among values ($P < 0.05$) (one-way ANOVA followed by Tukey's HSD test)

greater against *P. aeruginosa* than MRSA. The zone of inhibition against *P. aeruginosa* was 10, 15 and 20 mm at 25, 50 and 100 μg mL^{-1}, respectively. On the other hand, the zone of inhibition against MRSA was 8, 15 and 18 mm at 25, 50 and 100 μg mL^{-1}, respectively. However, bare chitosan showed inhibition zone of 5, 7 and 10 mm against MRSA and 5, 8 and 12 mm against *P. aeruginosa* at 25, 50 and 100 μg mL^{-1}, respectively. Bare $AgNO_3$ showed 5, 7 and 9 mm against MRSA and 5, 8 and 10 mm against *P. aeruginosa* at 25, 50 and 100 μg mL^{-1}, respectively. The positive control (Methicillin) displayed no activity against MRSA (Table 2). The antibacterial activities of AgNPs against Gram-negative bacteria were found to be higher than those of Gram-positive bacteria, which was consistent with the previous reports [36]. The difference between Gram-positive and Gram-negative bacteria is mainly the thickness of peptide glycan layer in their cell wall [36, 37]. These results indicate that the lower efficacy of the prepared Ch-AgNPs against Gram-positive bacteria species might be due to their thicker cell walls. In the present study, the size of inhibition zone was different among pathogens and the inhibition size increased as the concentration of Ch-AgNPs was increased. This was in agreement with Wei et al. [34] who stated that chitosan-based silver nanoparticles showed higher antibacterial activity towards *E. coli, S. aureus,* and *B. subtilis* compared to the ionic silver antibacterial activity for certain strains (*E. coli and S. aureus*). It has been documented that the chitosan has antimicrobial activity due to its cationic properties that cause a membrane disrupting effect [34]. The increased antimicrobial activity of Ag-incorporated (silver ions or nanoparticles) chitosan materials is due to the infiltrating ability of silver component resulting in a higher bactericidal effect.

Antibacterial Activity of Ch-AgNPs Coated Clinical Band-Aid Cloth (Cheese Cloth)

The antibacterial activity of uncoated and Ch-AgNPs coated clinical band-aid cloth was determined by measuring the inhibition zones formed around the clinical band-aid cloths. The zone of inhibition formed against *P.*

Table 2 Antibacterial activity of Ch-AgNPs in comparison with bare chitosan, bare $AgNO_3$ and methicillin

S. no.	Bacteria	Concentration ($\mu g\ mL^{-1}$)	Zone of inhibition (mm)*			
			Bare chitosan	Bare $AgNO_3$	Methicillin	Ch-AgNPs
1.	Methicillin resistant *Staphylococcus aureus* (MRSA)	25	5 ± 1.8^a	5 ± 1.8^a	0	8 ± 1.9^a
		50	7 ± 1.4^b	7 ± 1.4^b	0	15 ± 1.0^b
		100	10 ± 1.8^c	9 ± 1.1^c	0	18 ± 0.6^c
2.	*Pseudomonas aeruginosa*	25	5 ± 1.3^a	5 ± 1.8^a	–	10 ± 1.8^a
		50	8 ± 1.1^b	8 ± 1.0^b	–	15 ± 1.2^b
		100	12 ± 0.4^c	10 ± 0.9^c	–	20 ± 0.2^c

* Values are mean ± SE of three replicates. Within each column, different letters indicate significant differences among values ($P < 0.05$) (one-way ANOVA followed by Tukey's HSD test)

aeruginosa (Fig. 6A) and MRSA (Fig. 6B) and with bare chitosan coated (Fig. 6A, B) and Ch-AgNPs coated (Fig. 6A1, B1) clinical band-aid cloths are shown in Table 3. It is clear from the observed images that the Ch-AgNPs coated clinical band-aid cloths showed efficient antibacterial activity against MRSA and *P. aeruginosa* at

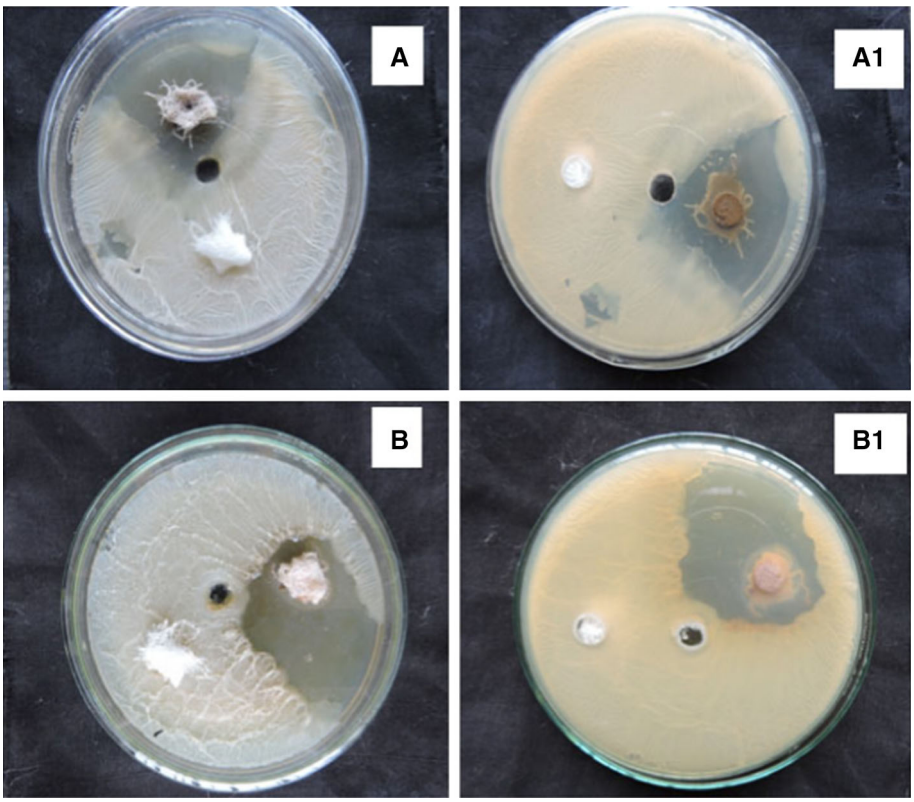

Fig. 6 In vitro antibacterial activity of Ch-AgNPs coated (100 $\mu g\ mL^{-1}$) and uncoated clinical band-aid cloth against Gram-negative *P. aeruginosa* (top panel; **A**, **A1**) and Gram-positive methicillin-resistant *S. aureus* (bottom panel; **B**, **B1**). **A**—Bare chitosan, A1-Ch-AgNPs; **B**—Bare chitosan, B1-Ch-AgNPs

Table 3 Antibacterial activity of Ch-AgNPs coated clinical band-aid cloth in comparison with bare chitosan, bare $AgNO_3$ and methicillin

S. no.	Bacteria	Concentration ($\mu g\ mL^{-1}$)	Zone of inhibition (mm)*			
			Bare chitosan	Bare $AgNO_3$	Methicillin	Ch-AgNPs
1.	Methicillin resistant *Staphylococcus aureus* (MRSA)	100	15 ± 1.0^a	10 ± 1.6^a	0	22 ± 0.8^a
2.	*Pseudomonas aeruginosa*	100	18 ± 1.1^b	12 ± 1.8^b	–	25 ± 0.5^b

* Values are mean ± SE of three replicates. Within each column, different letters indicate significant differences among values ($P < 0.05$) (one-way ANOVA followed by Tukey's HSD test)

100 μg mL^{-1}, while no inhibition zone was observed in control (uncoated clinical band-aid cloths). A recent report on the usage of silver nanoparticles for wound healing showed the importance of silver nanoparticles in bactericidal effect [25].

Antibiofilm Assay

The total biofilm biomass and total bacterial cell number in the biofilm were evaluated under confocal laser scanning microscope (CLSM). CLSM 3D view showed strong biofilm formation of MRSA (Supplementary Fig. S2A) and *P. aeruginosa* (Supplementary Fig. S2B) in control, whereas, Ch-AgNPs treatment (100 μg mL^{-1}) reduced biofilm formation. A significant reduction in the biofilm growth to about 65% and 75% was observed at 100 μg $mL^{-1}$of Ch-AgNPs against MRSA and *P. aeruginosa*, respectively (Fig. 7). The thickness of biofilm was also reduced to 7 mm and 9 mm after treatment with 100 μg mL^{-1} of Ch-AgNPs against MRSA and *P. aeruginosa,* respectively compared to control (16 and 30 mm respectively). However, bare $AgNO_3$ effectively inhibited the biofilm formation of MRSA at 250 μg mL^{-1} and *P. aeruginosa* at 150 μg mL^{-1} (data not shown). On the other hand, bare chitosan showed the least activity on the biofilm formation of MRSA and *P. aeruginosa* at the tested concentration (250 μg mL^{-1}) (data not shown). Ag is generally used as nitrate salt but in the form of Ag nanoparticles (AgNPs), the surface area tends to increase, which could be the underlying reason behind the enhanced antimicrobial efficacy [38]. It was reported that the biologically synthesized silver nanoparticles exhibit a potential antibiofilm activity against *P. aeruginosa* and *S. epidermidis* during 24 h treatment [39]. Our results are supported by the findings of Namasivayam and Roy [31] who reported that the chitosan stabilized chemogenic silver nanoparticles enhanced antibiofilm activity against *E. coli*. Jena et al. [21] reported that the increased antibiofilm effect of chitosan stabilized metallic nanoparticles may be due to the inhibition of exopolysaccharide synthesis limiting the formation of biofilm or due to diffusion of CS-AgNPs through the channels present in the biofilms followed by the sustained release of metal nanoparticles, which may impart antimicrobial functions.

Extracellular Polymeric Substance (EPS) Quantification Assay

Exopolysaccharide plays an important role in bacterial host cell interactions and biofilm architectures in microbes [40]. In the present study, 100 μg mL^{-1} of Ch-AgNPs effectively reduced the EPS production of MRSA (40%) and *P. aeruginosa* (70%) compared to control (Fig. 8). Our results

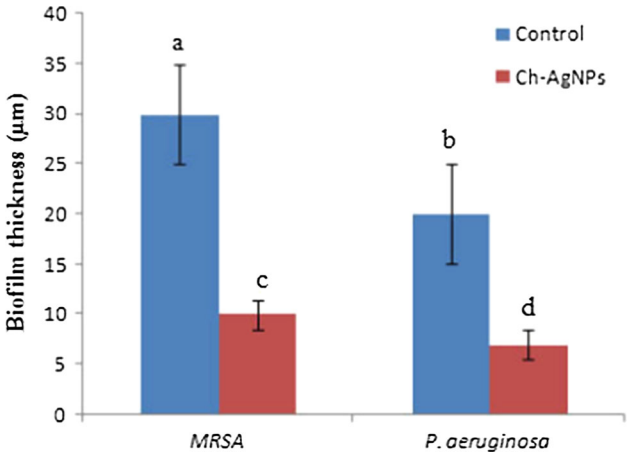

Fig. 7 Thickness of biofilm growth of Gram-positive methicillin-resistant *S. aureus* (a and c) and Gram-negative *P. aeruginosa* (b and d) in control (a and b) and 100 μg mL^{-1} Ch-AgNPs treatment (c and d). Ch-AgNPs treatment reduced the biofilm thickness of MRSA and *P. aeruginosa*

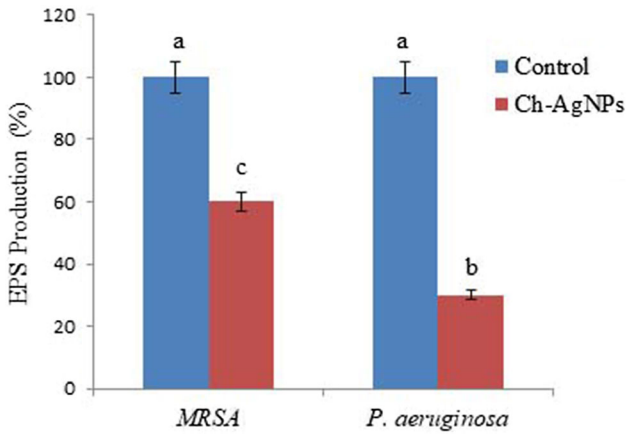

Fig. 8 Extracellular polymeric substances (EPS) production of Gram-positive methicillin-resistant *S. aureus* (c) and Gram-negative *P. aeruginosa* (b) after treatment with 100 μg mL^{-1} Ch-AgNPs compared to control (a)

corroborate the findings by Manju et al. [41] who reported that the hydrophobicity inhibition of *P. aeruginosa* and *S. aureus* by NsEO-AuNPs was 78% and 46%, respectively. Vaseeharan et al. [42] reported that the chitosan zinc composite blocked the production of EPS in *B. licheniformis* inhibiting biofilm formation.

Biofilm Detachment Assay

The effect of Ch-AgNPs on the detachment of MRSA and *P. aeruginosa* biofilm was evaluated in the presence of a surfactant. Quantification of bacterial biofilm was performed in the Ch-AgNPs (100 μg mL^{-1}) treated cells and control cells after the addition of SDS. As shown in Fig. 9A, B, SDS detached bacterial cells from both Ch-

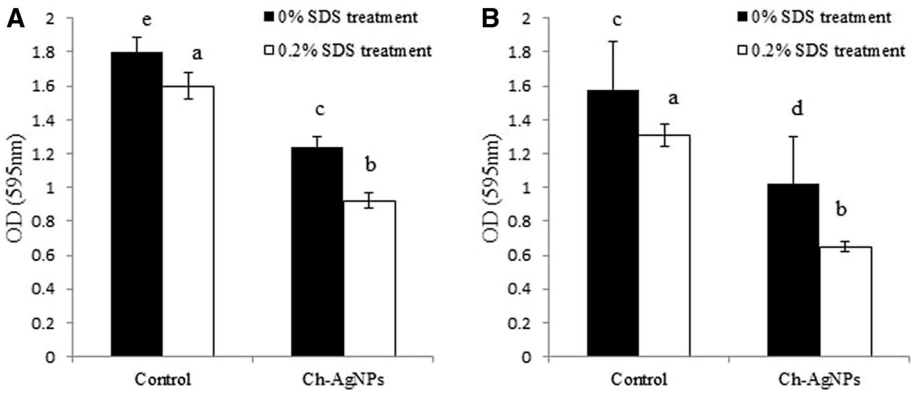

Fig. 9 Effect of Ch-AgNPs on the detachment of biofilms of **A** Gram-positive methicillin-resistant *S. aureus*, **B** Gram-negative *P. aeruginosa* in control and Ch-AgNPs treatment. Treatment with Ch-AgNPs at 100 μg mL^{-1} reduced the biofilm detachment

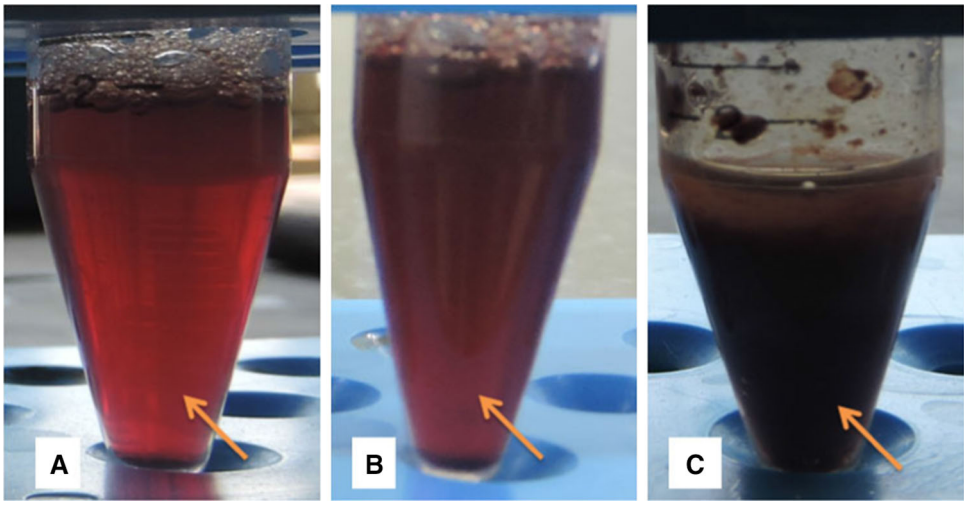

Fig. 10 Anticoagulant activity of Ch-AgNPs. Tube **A** has the blood collected with anticoagulant and Tube **B** has the blood collected with Ch-AgNPs. Arrow indicates the inhibition of blood clot formation. Tube **C** shows the blood clot formed. Arrow indicating the clotting without any anticoagulant

AgNPs treated cells and control cells. However, high detachment efficiency of 69% and 85% was observed in Ch-AgNPs treated group for MRSA and *P. aeruginosa,* respectively.

Anticoagulant Assay

The ultimate objective of preparing any nanoparticles is to provide significantly enhanced antimicrobial activity at least concentrations as possible, without any adverse effect in humans. Here, due to the excellent biological activity of the synthesized Ch-AgNPs, we examined the anticoagulation property using human blood plasma. Anticoagulants are used to treat or prevent blood clots including prevention of recurrent clots, pulmonary embolism, and death. Previous reports revealed an enhanced anti-platelet property of nanosilver in mouse model in vivo [29, 43]. The anticoagulant activity of the synthesized Ch-AgNPs was compared with those of heparin (commercial anticoagulant) (Fig. 10A). The results revealed that Ch-AgNPs exhibited anticoagulant activity as equivalent to the commercial anticoagulant heparin (Fig. 10B). The results are in conformity to those reported in the previous study that the anti-inflammatory property of either gold or silver heparin nanoparticles showed a negligible effect on systemic homeostasis upon the administration in carrageenan-induced paw edema models [44–46].

Conclusion

The current study reports the development of silver nanoparticles using shrimp shell chitosan. The particle size, functional groups and morphology of the synthesized Ch-AgNPs were investigated using UV–Vis, XRD, FTIR, HR-TEM with EDX measurements. The size of Ch-AgNPs ranges between 10 and 50 nm and are moderately stable. The EDX and XRD pattern of the synthesized Ch-AgNPs confirmed the purity and crystalline nature of the particles. FTIR showed the possible biomolecules involved in the reduction of $AgNO_3$ to AgNPs. Ch-AgNPs showed effective antibacterial action and control of MRSA and *P. aeruginosa* bacterial biofilms. Furthermore, Ch-AgNPs showed high biofilms detachment activity against Gram-negative *P. aeruginosa* compared to Gram-positive MRSA. Also, the biofilm formed in the presence of Ch-AgNPs

detached more easily with surfactant than those without Ch-AgNPs. Ch-AgNPs displayed excellent biocompatibility by exhibiting anticoagulant activity against human blood clots. In addition, Ch-AgNPs coated clinical band-aid cloth showed enhanced antibacterial activity against MRSA and *P. aeruginosa*. The obtained findings the use of dressings with Ch-AgNPs may either inhibit or diminish microbial development in the wound atmosphere, and reducing wound bioburden may recover wound-healing outcomes, and powerfully recommend the Ch-AgNPs use of the industrialized novel nano material dressing for wound care applications.

Acknowledgements The First author S. Vijayakumar (SRF) thanks the DST, New Delhi, India for financial support under INSPIRE programme (INSPIRE Fellow-IF140145). The authors thank the RUSA phase 2.0 Grant [Ref-24-51-2014-U policy] TN Multi-Gen. Department of Education, Government of India. The authors gratefully acknowledge the Alagappa University, University Scientific Instrumentation Centre (USIC) for providing Confocal laser scanning microscopy, XRD and FTIR instrumental facilities to this research. Mr. S. Vijayakumar acknowledges the help of Mrs. Marry, Nurse, Govt. hospital, Karaikudi, Tamil Nadu, India for blood sample collection.

Compliance with ethical standards

Conflict of interest The authors report no conflict of interest.

References

1. R. S. Kirsner, H. Orstead, and J. B. Wright (2001). *Wounds.* **13**, 5–12.
2. S. L. Percival, S. M. McCarty, and B. Lipsky (2015). *Adv. Wound Care.* **4**, 373–381.
3. S. S. Grant and D. T. Hung (2013). *Virulence.* **4**, 273–283.
4. C. E. Black and J. W. Costerton (2010). *Surg. Clin. N. Am.* **90**, 1147–1160.
5. S. Finnegan and S. L. Percival (2015). *Adv. Wound Care* **4**, 398–406.
6. R. Edwards and K. G. Harding (2004). *Curr. Opin. Infect. Dis.* **17**, (2), 91–96.
7. L. Scrivano, D. Iacopetta, M. S. Sinicropi, C. Saturnino, P. Longo, O. I. Parisi, and F. Puoci (2017). *Drug Deliv.* **24**, 482–490.
8. R. Jayakumar, M. Prabaharan, and R. A. A. Muzzarelli (2011). *Adv. Polym. Sci.* **243**, 23–54.
9. M. Dash, F. Chiellini, R. M. Ottenbrite, and E. Chiellini (2011). *Prog. Polym. Sci.* **36**, 981–1014.
10. M.I.Z. Lionzo, A.C. Dressler, O. Mertins, A.R. Pohlmann and N.P. da Silveira, in *Nanocosmetics and Nanomedicines* (2011), pp. 163–174 (Chapter 8).
11. M. Kong, X. G. Chen, K. Xing, and H. J. Park (2010). *Int. J. Food Microbiol.* **144**, 51–63.
12. R. Jayakumar, M. Prabaharan, P. T. Sudheesh Kumar, S. V. Nair, and H. Tamura (2011). *Biotechnol. Adv.* **29**, 322–337.
13. X. Chen and H. J. Schluesener (2008). *Toxicol. Lett.* **176**, 1–12.
14. S. Vijayakumar, B. Malaikozhundan, N. Gobi, B. Vaseeharan, and C. Murthy (2016). *Limnologica.* **61**, 44–51.
15. D. Bagal-Kestwal, R. M. Kestwal, W. T. Hsieh, and B. H. Chiang (2014). *J. Pharm. Biomed. Anal.* **88**, 571–578.
16. B. Ankamwar, M. Chaudhary, and M. Sastry (2005). *Metal Organic Nano Metal Chem.* **35**, 19–26.
17. S. Shankar, A. Absar, and S. Murali (2003). *Biotech. Prog.* **19**, 1627–1631.
18. M. Ali, N. Thajuddin, K. Jeganathan, and M. Gunasekaran (2011). *Colloids Surf. B.* **85**, 360–365.
19. S. P. Chandran, M. Chaudhary, R. Pasricha, A. M. Ahmad, and M. Sastry (2006). *Biotech. Prog.* **22**, 577–583.
20. V. Deepak, P. S. Umamaheshwaran, K. Guhan, R. A. Nanthini, B. Krithiga, N. M. H. Jaithoon, and S. Gurunathan (2011). *Colloids Surf. B.* **86**, 353–358.
21. P. Jena, S. Mohanty, R. Mallick, B. Jacob, and A. Sonawane (2012). *Int. J. Nanomed.* **7**, 1805–1818.
22. L. Wang, C. C. Liu, Y. Yan Wang, H. Xu, H. Su, and X. Cheng (2016). *Curr. Appl. Phys.* **16**, 969–973.
23. C. Perez, M. Paul, and P. Bazerque (1990). *Acta Biol. Med. Exp.* **15**, 113–135.
24. CLSI, *Methods for Dilution Antimicrobial Susceptibility Tests for Bacteria That Grow Aerobically* (2012) **32**, 69.
25. A. Sankaranarayanan, G. Munivel, G. Karunakaran, S. Kadaikunnan, N. S. Alharbi, N. J. M. Khaled, and D. Kuznetsov (2017). *J. Clust. Sci.* **28**, 995–1008.
26. B. Malaikozhundan, B. Vaseeharan, S. Vijayakumar, R. Sudhakaran, N. Gobi, and G. Shanthini (2016). *Biocatal. Agric. Biotechnol.* **8**, 189–196.
27. S. Favre-Bonte, T. Kohler, and C. J. Van Delden (2003). *Antimicrob. Chemother.* **52**, 598–604.
28. D. G. Davies, M. R. Parsek, J. P. Pearson, B. H. Iglewski, J. W. Costerton, and E. P. Greenberg (1998). *Science.* **280**, 295–298.
29. K. Kalishwaralal, V. Deepak, S. R. Pandian, M. Kottaisamy, S. BarathManiKanth, B. Kartikeyan, and S. Gurunathan (2010). *Colloids Surf. B.* **77**, 257–262.
30. S. K. Balavandy, K. Shameli, and Z. Z. Abidin (2015). *Int. J. Electrochem. Sci.* **10**, 486–497.
31. S. K. R. Namasivayam and E. A. Roy (2013). *Int. J. Sci. Res. Pub.* **3**, 1–9.
32. P. Patel, P. Agarwal, S. Kanawaria, S. Kachhwaha, S. Kothari, in *Nanotechnology and Plant Sciences* (2015), pp. 271–288.
33. H. V. Tran, L. Dai Tran, C. T. Ba, H. D. Vu, T. N. Guyen, D. G. Pham, and P. X. Nguyen (2010). *Colloids Surf. A Physicochem. Eng. Aspects.* **360**, 32–40.
34. A. Wei, W. Sun, W. Qian, Y. Ye, and X. Ma (2009). *Carbohydr. Res.* **344**, 2375–2382.
35. S. D. S. Lima, B. Gullon, A. Cardelle-Cobas, L. M. Brito, K. A. F. Rodrigues, P. V. Quelemes, J. Ramos-Jesus, D. D. R. Arcanjo, A. Placido, K. Batziou, P. Quaresma, P. Eaton, C. Delerue-Matos, F. A. A. Carvalho, D. A. Silva, M. Pintado, and J. R. S. A. Leite (2017). *J. Bioact. Compat. Polym.* **32**, 397–410.
36. P. Kanmani and T. L. Seung (2013). *Process Biochem.* **48**, 1099–1106.
37. S. Priyadarshini, V. Gopinath, N. Meera Priyadharsshini, D. MubarakAli, and P. Velusamy (2013). *Colloid Surf. B.* **102**, 232–237.
38. J. S. Kim, J. S. Kuk, K. Yu, J. H. Kim, S. J. Park, H. J. Lee, S. H. Kim, Y. K. Park, Y. H. Park, C. Y. Hwang, Y. K. Kim, Y. S. Lee, D. H. Jeong, and M. H. Cho (2007). *Nanomedicine.* **3**, 95–101.
39. V. Arya, R. Komal, M. Kaur, and A. Goyal (2011). *Pharmacologyonline* **3**, 118–124.
40. E. Borghi, R. Sciota, C. Biassoni, D. Cirasola, L. Cappelletti, L. Vizzini, P. Boracchi, and G. Morace (2011). *J. Med. Microbiol.* **60**, 689–690.

41. S. Manju, B. Malaikozhundan, S. Vijayakumar, S. Shanthi, A. Jaishabanu, P. Ekambaram, and B. Vaseeharan (2016). *Microb. Pathog.* **91**, 129–135.
42. B. Vaseeharan, J. Sivakamavalli, and R. Thaya (2015). *J. Compos. Mater.* **49**, 177–184.
43. M. M. Kemp, A. Kumar, S. Mousa, T. J. Park, P. Ajayan, N. Kubotera, S. A. Mousa, and R. J. Linhardt (2009). *Biomacromolecules.* **10**, 589–595.
44. M. Jeyaraj, S. Varadan, K. J. P. Anthony, M. Murugan, A. Raja, and S. Gurunathan (2013). *J. Ind. Eng. Chem.* **19**, 1299–1303.
45. M. Schäfer and S. Werner (2008). *Pharmacol. Res.* **58**, 165–171.
46. P. Pallavicini, C. R. Arciola, F. Bertoglio, S. Curtosi, G. Dacarro, A. Dagostino, F. Ferrari, D. Merlili, C. Milanese, S. Rossi, A. Taglietti, M. Tenci, and L. Visai (2017). *J. Colloid Interface Sci.* **15**, 271–281.